AD-A041 777 TECHNION - ISRAEL INST OF TECH HAIFA MATERIAL MECHAN--ETC F/G 11/10
NONLINEAR ANELASTIC BEHAVIOR OF A SYNTHETIC RUBBER AT FINITE ST--ETC(U)
MAR 77 D DERMAN, Z ZAPHIR, S R BODNER AF-AFOSR-2607-74
UNCLASSIFIED MML-53 AFOSR-TR-77-0721 NL

| OF |
AD
A041777

END

DATE
FILMED
8-77

NONLINEAR ANELASTIC BEHAVIOR OF A SYNTHETIC RUBBER AT FINITE STRAINS

by

D. DERMAN, Z. ZAPHIR AND S. R. BODNER

MML Report No. 53

March 1977

המעבדה למכניקת החומרים
הפקולטה להנדסת מכונות
הטכניון — מכון טכנולוגי לישראל

TECHNION—ISRAEL INSTITUTE OF TECHNOLOGY
FACULTY OF MECHANICAL ENGINEERING
MATERIAL MECHANICS LABORATORY
HAIFA, ISRAEL

Scientific Report No. 11
ROARD, USAF
Grant AFOSR-74-2687

AIR FORCE OFFICE OF SCIENTIFIC RESEARCH (AFSC)
NOTICE OF TRANSMITTAL TO DDC
This technical report has been reviewed and is
approved for public release IAW AFR 190-12 (7b).
Distribution is unlimited.
A. D. BLOSE
Technical Information Officer

Grant AFOSR-74-2607

(11) March 1977

SCIENTIFIC REPORT NO. 11

(12) 36p.

(6) NONLINEAR ANELASTIC BEHAVIOR OF A SYNTHETIC RUBBER AT FINITE STRAINS

(18) AFOSR

(19) TR-77-0721

by

(10) D./DERMAN,
Z./ZAPHIR
and S.R./BODNER

(15) AF-AFOSR-2607-74

(14) MML [redacted]-53, Scientific-11

Material Mechanics Laboratory
Faculty of Mechanical Engineering
Technion - Israel Institute of Technology
Haifa, Israel

The research reported in this document has been supported in part by the AIR FORCE OFFICE OF SCIENTIFIC RESEARCH under Grant AFOSR-74-2607, through the European Office of Aerospace Research and Development (EOARD), United States Air Force.

401 910

1B

NONLINEAR ANELASTIC BEHAVIOR OF A SYNTHETIC RUBBER AT FINITE STRAINS

by

D. Derman[1], Z. Zaphir[2], and S. R. Bodner[3]

Faculty of Mechanical Engineering
Technion - Israel Institute of Technology

Abstract

A set of constitutive equations has been developed to represent nonlinear anelastic behavior, i.e. energy losses and rate dependent moduli for geometrically large, reversible deformations. These equations are in incremental form and can be used to solve boundary value problems by numerical methods. Two problems were considered: thick walled spheres subjected to cycles of internal pressure, and a long rod subjected to imposed axial velocity (the simple tension test). Experiments were carried out for both conditions on specimens made of a synthetic rubber at three different temperatures (each under isothermal conditions) and at different loading rates. Response curves were calculated based on the constitutive equations and chosen values of the material constants. Generally good agreement was obtained between the predicted and experimental results.

---

[1]Graduate Student (formerly)

[2]Graduate Student

[3]Professor

Introduction

Theories of nonlinear viscoelasticity have been proposed in recent years to account for various nonlinear geometrical and material effects associated with time dependent deformations (summarized by Lockett in [1,2]). These theories generally reduce to classical linear viscoelasticity as the limiting condition for small deformations. Linear viscoelasticity can be placed on a firm axiomatic foundation, Gurtin and Sternberg [3], and has been extensively developed, but the theoretical bases of the nonlinear theories are still in a general state, e.g. Rivlin [4], and detailed development and practical application of the theories have been slow.

An alternative to specialization of a general theory for practical representation is to consider particular classes of material response guided by physical considerations and overall theoretical constraints. The present paper is concerned with a nonlinear representation of "anelastic" behavior defined slightly more generally than by Zener [5] as geometrical reversible deformation with energy loss. That is, the deformations are reversible so that the original geometrical state is recovered upon unloading but the loading and unloading paths do not coincide, i.e., the cycle is not thermodynamically reversible. This class of material response has received considerable attention since the energy loss for small amplitude reversible deformations is the well known "internal damping" of materials. Linear viscoelasticity is generally used to represent internal damping for small oscillations and extensive studies have been made to relate the parameters in the linear equations to physical energy dissipation mechanisms in metals and plastics.

Relatively little work has been done, however, on formulating anelastic behavior in the nonlinear range. This paper describes a procedure for representing nonlinear anelasticity which is similar to one developed for inelastic (non-reversible) deformations by Partom and Bodner [6,7,8]. The constitutive equations consider the increments of both the reversible and the non-reversible deformation rate components to be functions of state quantities and the current geometry. The changes in the state quantities with deformation are given by suitable evolutionary equations. In this manner, the material response to arbitrary loading or straining histories is calculable on a step by step basis. Anelastic behavior can be considered in a similar manner by an anelastic stress term, not a state variable, which is a nonlinear function of the total deformation rate and state quantities. Only reversible deformations are considered in the present paper but generally both anelasticity and inelasticity can be treated simultaneously.

Since the deformations are reversible and the total stress is considered to be decomposable into elastic and anelastic components, the present formulation is essentially equivalent to a nonlinear generalization of the Kelvin-Voigt viscoelastic model. Nonlinearity is introduced in the elastic element through the use of a general nonlinear stress-strain relation whose coefficients are derived from a strain energy function and by the inclusion of a finite strain measure. The anelastic stress is a nonlinear function of the deformation rate as well as a function of the elastic stress. One of the consequences of this approach is that the effective "dynamic modulus" and "damping" become uncoupled so their frequency dependence could be specified separately which is essentially different than linear viscoelastic

theory.

Lockett in [1,2] classified nonlinear viscoelasticity as a consequence of various effects: "magnitude," i.e. stress and strain amplitude, "interaction," i.e. different times of load application, and "intermode," i.e. changes in direction of load application. In his terminology, the present formulation attempts to treat both magnitude and interaction nonlinearity. Intermode nonlinearity is also implied but only investigated insofar as two different boundary value problems are treated. There are a large number of interaction effects which could be examined, such as superimposed loading during creep or recovery, and Lockett has developed a modified Kelvin-Voigt model to treat such problems [9]. The interaction examples in this paper are limited to the frequency dependence of the load-elongation relation during loading and unloading cycles.

A brief review of the theoretical development of the nonlinear anelastic formulation was presented in [10] where some results were also given for thick walled hollow spheres subjected to loading and unloading cycles of internal pressure under quasi-static and isothermal conditions. This paper gives a more complete presentation of the basic formulation and describes and discusses the sphere results in greater detail. These spheres were prepared from a synthetic rubber and were tested at various frequencies and temperatures. In addition, an extensive study was made on the same material for the uniaxial loading condition based on the same constitutive equations and material constants. Both analytical and experimental results for this case were obtained and are discussed in this paper.

Nonlinear Anelastic Model

A general set of constitutive equations to represent inelastic and anelastic material behavior at finite strains was initially proposed by Partom [11]. These were subsequently developed by Partom and Bodner in a series of papers [6,7,8] to apply to the elastic-plastic and viscoplastic response of both non-hardening and strain hardening materials. In this general formulation, the deformation rate,

$$d_{ij} = (1/2)(v_{i,j} + v_{j,i}) \tag{1}$$

where v_i is the particle velocity, is assumed decomposable into geometrically reversible and non-reversible components, d^e_{ij} and d^p_{ij}. The stress is taken to have an anelastic component σ^a_{ij} to account for energy losses (hysteresis) in reversible motions due to internal non-homogeneities. The elastic stress σ^e_{ij} is a state quantity. Under these assumptions, the rate of work per unit of current volume can be expressed as

$$\dot{W} = (\sigma^e_{ij} + \sigma^a_{ij})(d^e_{ij} + d^p_{ij}) \tag{2}$$

The deformation rate components and the anelastic stress are considered to be functions of state variables, e.g. σ^e_{ij}, T, and the velocity field. All history and memory effects are therefore included in the current state quantities and the geometry so that problems could be solved on a direct incremental basis in time. This makes the formulation readily adoptable to the computer solution of boundary value problems.

In the present treatment of anelastic materials, the non-reversible deformation rate d^p_{ij} is taken to be identically zero although, in principle, both anelastic and inelastic effects could be considered simultaneously. The problem therefore reduces to determining suitable expressions for d^e_{ij} (subsequently identified as d_{ij}) and for σ^a_{ij}.

Firstly, suitable constitutive equations are obtained for d^e_{ij} as a function of the elastic stress σ^e_{ij} on the basis of non-linear (large deformation) elasticity theory. Using the Almansi finite strain measure, the relation between the strain rate and the deformation rate is given by [6, 12]

$$\dot{\varepsilon}_{ij} = d_{ij} - (\varepsilon_{\alpha i} v_{\alpha,j} + \varepsilon_{\alpha j} v_{\alpha,i}) \tag{3}$$

where ε_{ij} denotes the total strain. A general expression for the elastic "true" stress-strain relationship is, from [6] and [14],

$$\sigma^e_{ij} = F_0 \delta_{ij} + F_1 \varepsilon_{ij} + F_2 \varepsilon_{\alpha i} \varepsilon_{\alpha j} \tag{4}$$

where the coefficients are obtained from strain energy functions (as described in [6]). Eq. (4) together with the strain energy functions and the strain rate expression, Eq. (3), would then define the elastic constitutive equations. An uncoupled form of the strain energy function was developed in [13] and used subsequently in [6] and [7]. Since the details of the development and the resulting constitutive equations are given essentially in [6] and [7], they will not be repeated here.

Modifications to the previous work were required, however, to obtain adequate representation in certain cases. In [6] and [7], the expression for the distortional energy, which is taken to be uncoupled from the dilatational energy, is written in terms of the Almansi strain invariants, E_1, E_2, as

$$W_s = 6\mu_0 (E_1^2 - 3E_2)/(3 - 2E_1)^2 \tag{5}$$

where μ_0 is the classical elastic shear modulus (see also [14]). Eq. (5) is a particular case of a more general form for W_s based on the shear energy being homogeneous of degree zero in the principal extensions, namely

$$W_s = C \left\{ \frac{\alpha_1(3-2E_1)^2 + \alpha_2(3-4E_1+4E_2)}{\beta_1(3-2E_1)^2 + \beta_2(3-4E_1+4E_2)} \right\} \tag{6}$$

where C and the α's and β's are constants. In order for the shear energy to vanish for pure dilatation, $3\alpha_1 + \alpha_2 = 0$, and to avoid singularities, $3\beta_1 + \beta_2 \neq 0$. In addition, for small strains W_s should reduce to the classical value $(-2\mu_0 \underline{E}_2)$. For α_1 set equal to unity as a common factor, these conditions lead to $\alpha_2 = -3$ and $\beta_2 = (1-9\beta_1)/3$ so that W_s reduces to

$$W_s = 2\mu_0 \left\{ \frac{E_1^2 - 3E_2}{3 - 4E_1 + 12\beta_1 E_1^2 + 4(1-9\beta_1)E_2} \right\} \tag{7}$$

Eq. (5) is obtained from Eq. (7) by setting $\beta_2 = 0$ (i.e. $\beta_1 = 1/9$) which was found adequate for strains up to about 15 to 30% (depending on test temperature). For strains as high as 50 to 100%, it was found that nonzero values of β_2 led to better overall representation of the experimental results.

Another modification to the strain energy function was to introduce weak coupling between the shear and dilatational energies. This can be done by considering the shear modulus μ to depend on the density change due to compressibility, i.e.

$$\mu = \mu_0 (s_0)^{\gamma} \tag{8}$$

where

$$s_0^2 = (\rho/\rho_0)^2 = 1-2E_1 + 4E_2 - 8E_3 \tag{9}$$

and (ρ/ρ_0) is the ratio of current to initial density and the E's are the Almansi strain invariants. For the material and conditions examined, γ could be set equal to zero in most cases but not all. For completeness, it is noted that the expression used for the dilatational energy, as in [6] and [7], is

$$W_v = \frac{9}{4} \frac{K_0}{\alpha(\beta-\alpha)} \left[(1-s_0)^{\frac{2}{3}\alpha} - \frac{\alpha}{\beta}(1-s_0)^{\frac{2}{3}\beta}\right] \tag{10}$$

where K_0 is the bulk modulus and α and β are constants that determine the variation of compressibility with pressure. As in the previous work, we used $\alpha = 1$ and $\beta = 2$.

The elastic shear modulus μ_0 was taken to be a constant independent of temperature over the range of temperatures in which the material behaves in a viscoelastic manner. That is, the shear modulus value in the rubbery region was taken to be the constant value. Temperature variations were introduced in the parameters that make up the time dependence, i.e. in the expression for the anelastic stress, which leads to an inter-relationship between temperature and time which is generally

observed for polymeric materials. It was necessary, however, to consider K_0 to have some temperature dependence to correlate with the experimental data.

In the present analysis, the anelastic stress term σ_{ij}^a is specifically introduced to account for energy losses under geometrically reversible deformations. In addition, it should represent other effects such as rate dependent dynamic moduli and transient effects during creep and stress relaxation. Anelasticity is associated essentially with shear deformations so that the terms in the governing law should be the deviatoric components of stress and deformation rate.

General observations of anelastic effects in many materials indicate that the dynamic modulus increases with increasing frequency but that the damping factor, $\tan\delta$ or Q^{-1}, changes only slightly with frequency over a wide range except near a relaxation point. The damping factor is defined in the usual manner

$$\tan\delta = W_d/2\pi W_e \tag{11}$$

where W_d and W_e are respectively the dissipated and the maximum elastic energy in a cycle per unit original volume. Because of the above mentioned characteristics of real materials, the standard viscoelastic models, which specify an interrelation between the frequency dependence of the dynamic modulus and the damping, can only be fitted to experimental data in a narrow frequency band. The present formulation enables the damping and modulus changes with frequency to be expressed independently although some interaction results from the nonlinearity.

Making the anelastic stress term independent of time would lead to frequency independent energy losses. A proposed expression for the energy loss term is

$$(\underline{\sigma}^{a}_{ij})_1 = f \frac{\underline{d}_{ij}}{|d_{kk}|} \tag{12}$$

where f is a constant, the bar symbol indicates the deviatoric component, and $|d_{kk}|$ is the absolute value of the first invariant of the deformation rate (rate of volume change). Eq. (12) is similar to a Coulomb type dry friction and implies that the friction magnitude depends on the ratio of the deviatoric to the dilatational deformation rates. It is noted that dilatational deformations would always be present due to nonlinearity and possible coupling factors and experiments have shown that volume changes do influence the energy loss factor [15,16].

Rate dependent material response could be introduced by making σ^{a}_{ij} depend directly on σ^{e}_{ij} and the deformation rate. A proposed equation for this effect is

$$(\underline{\sigma}^{a}_{ij})_2 = \underline{\sigma}^{e}_{ij} \sum_{n=1}^{N} g_n \exp[-\alpha_n/(-\underline{D}_2)^{1/2}] \tag{13}$$

where g_n and α_n are constants and $\underline{D}_2$ is the second invariant of the deviatoric component of the deformation rate. Since $\underline{D}_2$ is a negative quantity, the minus sign is introduced to make the term $(-\underline{D}_2)$ positive. The series form of Eq. (13) is analogous to that used to express linear viscoelastic functions in order to approximate experimental results (Prony Series). Eq. (13) corresponds to an additional increment to the elastic stress whose magnitude increases with

deformation rate. Using only Eq. (13) in conjunction with the previous elastic equations would lead to a rate dependent nonlinear elasticity theory, i.e. the material response would be rate dependent but fully reversible without energy losses. The anelastic effects of importance in the present investigation are therefore given by Eq. (12), which provides for rate independent energy losses, and Eq. (13) for frequency dependent response. Coupling of these effects will occur, however, because of the essential nonlinearity of the formulation. The total expression for the anelastic stress term for the present problem is then

$$\underline{\sigma}^{a}_{ij} = f \frac{\underline{d}_{ij}}{|\underline{d}_{kk}|} + \underline{\sigma}^{e}_{ij} \sum_{n=1}^{N} g_n \exp[-\alpha_n/(-\underline{D}_2)^{1/2}] \qquad (14)$$

which is used in conjunction with the elastic stress-strain relations to give the set of constitutive equations for anelastic materials in the solution of boundary value problems. In these problems, the total stress in the equilibrium equations is the sum of the elastic and anelastic components.

The constitutive equations consisting of the elastic and anelastic terms were applied to compute the quasi-static response of thick walled spherical shells made from a synthetic rubber subjected to cycles of internal pressure at various frequencies and at three constant temperatures. A description of these experiments on spheres is given in the next section and a short review of the investigation has been presented [10]. In that application, the equilibrium equation was solved at each step in time at a number of points along the radial coordinate according to the required accuracy. The state (stresses, deformations, deformation rates) at the end of each time step were used

as the basis for the calculation of the new quantities at the next step.

For the uniaxial straining case, the same constitutive equations were applied to calculate the stress resulting from extension of a thin long rod of the same synthetic rubber. Tests and corresponding calculations were carried out for three imposed axial velocities at the same three temperatures. The calculations were initially based on the same equations and material constants used for the sphere problem. It was found, however, that the use of Eq. (5) for the shear strain energy limited the predictive capability of the calculations for the tensile straining problem to a maximum strain of about 30%. Eq. (5) is derived from the more general expression for W_s, Eqs. (6) and (7), by setting the constant $\beta_2=0$. Considering $\beta_2 \neq 0$ and using Eq. (7) for W_s in which $(1-9\beta_1) = 3\beta_2$ led to very good fitting of the uniaxial tests results for strains up to 100%. This change had very little effect on the calculations for the sphere problem over the range of interest. An auxiliary program was used to determine β_2 based on matching a given point on the stress-deformation curve for a particular crosshead velocity.

The Almansi strains for the uniaxial case are simply $\varepsilon_{ij} = (1/2)(1-\lambda_i^{-2})$ for $i=j$ and $\varepsilon_{ij} = 0$ for $i \neq j$ where the λ_i are the extension ratios. It is noted that the terms $|d_{kk}|$ and $\underline{D}_2$ in Eq. (14) could be expressed as functions of Poisson's Ratio since $d_{kk} = \mathring{\lambda}_1+\mathring{\lambda}_2+\mathring{\lambda}_3$ and $\underline{D}_2 = \mathring{\lambda}_1\mathring{\lambda}_2 + \mathring{\lambda}_2\mathring{\lambda}_3 + \mathring{\lambda}_3\mathring{\lambda}_1 - (1/3)d_{kk}^2$. For uniaxial straining, $\mathring{\lambda}_2 = \mathring{\lambda}_3 = -\nu\mathring{\lambda}_1$, so that $d_{kk} = \mathring{\lambda}_1(1-2\nu)$ and $\underline{D}_2 = -(1/3)\mathring{\lambda}_1^2(1+\nu)^2$.

The steps in the numerical procedure and the associated block diagram are given as follows:

Procedure Steps:

1. Input of geometric and material parameters and crosshead (imposed axial) velocity V.
2. Selection of a particular deformation value at which the computed and experimental values of the axial stress σ_1 are to be matched.
3. Calculation of β_1 by a triple phase Newton-Raphson iteration procedure using the following conditions:
   a) Equalizing the lateral stress to zero.
   b) Matching the computed axial stress value to the experimental at the deformation selected at step 2:

   $$\sigma_1(\lambda_1^{(0)}) = \sigma_1^{(exp)}(\lambda_1^{(0)})$$

   where $\lambda_1^{(0)}$ is the extension ratio at the matched point.
   c) Requiring the Poisson Ratio to be

   $$\nu = \left(\frac{\partial \lambda_2}{\lambda_2}\right) \Big/ \left(\frac{\partial \lambda_1}{\lambda_1}\right) \Big|_{\sigma_2=0}$$

4. Using the values of β_1 obtained in step 3, the axial stress, σ_1, is computed for a series of deformations $\lambda_1^{(i)}$ during loading and unloading using a double phase Newton-Raphson iteration procedure and applying the conditions (a) and (c) described above. The convergence is speeded up by the use of relaxation factors and using initial values based on results of the preceding steps.
5. Using the same value of β_1, step 4 is repeated for other imposed velocities.

The block diagram of the calculation procedure for uniaxial extension is given on the following page.

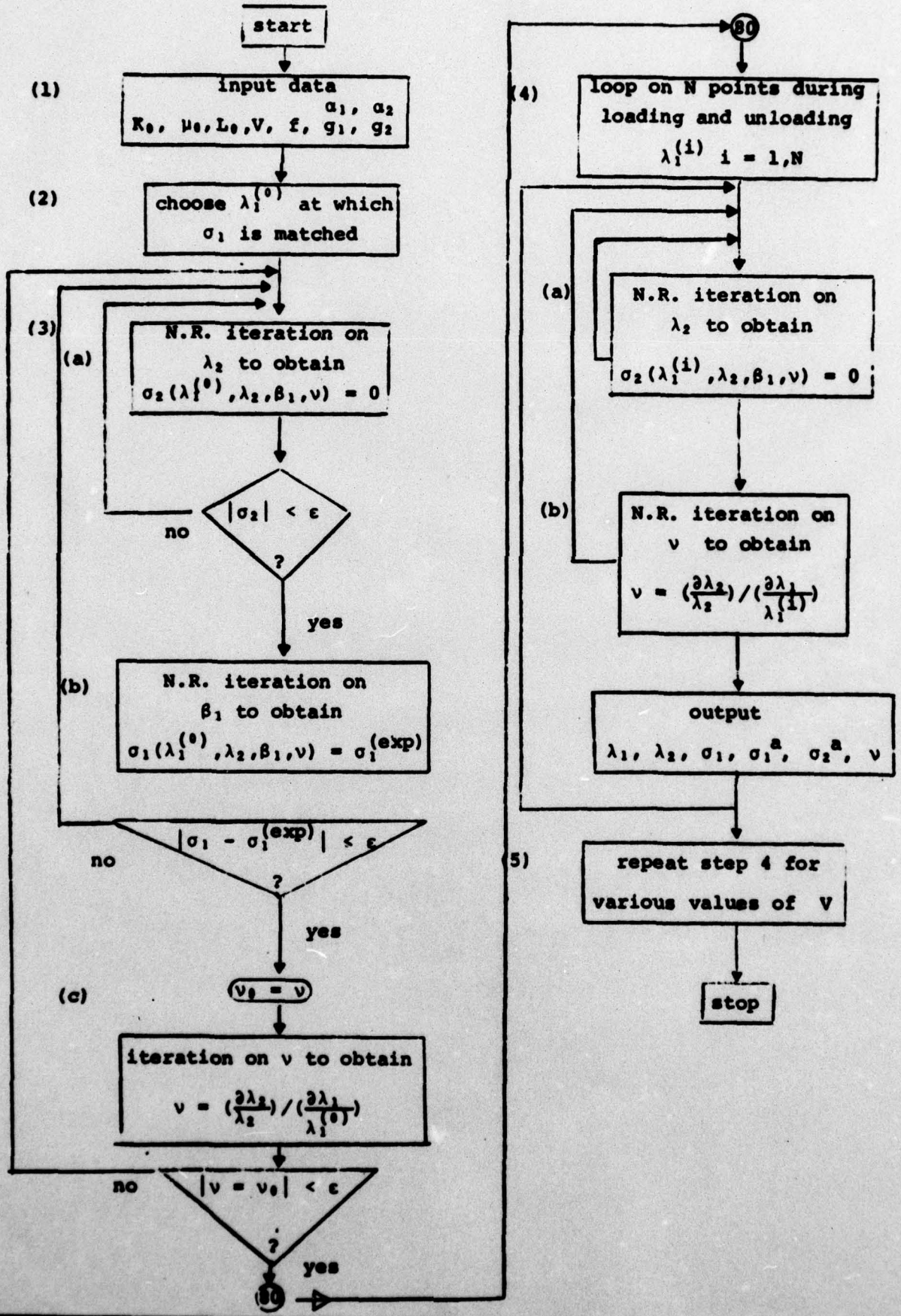
start
(1)
input data
α_1, α_2
K_0, μ_0, L_0, V, f, g_1, g_2
(2)
choose $\lambda_1^{(0)}$ at which σ_1 is matched
(3)
(a)
N.R. iteration on λ_2 to obtain $\sigma_2(\lambda_1^{(0)}, \lambda_2, \beta_1, \nu) = 0$
$|\sigma_2| < \varepsilon$?
no
yes
(b)
N.R. iteration on β_1 to obtain $\sigma_1(\lambda_1^{(0)}, \lambda_2, \beta_1, \nu) = \sigma_1^{(exp)}$
$|\sigma_1 - \sigma_1^{(exp)}| \leq \varepsilon$?
no
yes
(c)
$\nu_0 = \nu$
iteration on ν to obtain $\nu = (\frac{\partial \lambda_2}{\lambda_2}) / (\frac{\partial \lambda_1}{\lambda_1^{(0)}})$
$|\nu - \nu_0| < \varepsilon$?
no
yes
(30)
(30)
(4)
loop on N points during loading and unloading
$\lambda_1^{(i)}$ i = 1,N
(a)
N.R. iteration on λ_2 to obtain $\sigma_2(\lambda_1^{(i)}, \lambda_2, \beta_1, \nu) = 0$
(b)
N.R. iteration on ν to obtain $\nu = (\frac{\partial \lambda_2}{\lambda_2}) / (\frac{\partial \lambda_1}{\lambda_1^{(i)}})$
output
λ_1, λ_2, σ_1, σ_1^a, σ_2^a, ν
(5)
repeat step 4 for various values of V
stop

Experimental Procedure and Results

For the thick walled sphere problem, two sets of spheres having inner-outer diameters of 60 - 120 mm and 75 - 100 mm were fabricated of a synthetic rubber. To measure the inner radial displacement, a specially designed extensometer was embedded in the inner cavity prior to casting the sphere as a single piece. Another extensometer was attached to the outer surface. The spheres were subjected to rectified sinusoidal cycles of positive internal pressure by means of a servo controlled pressure system. The pressure and the inner and outer radial displacements were continually recorded.

Tests were run at a constant temperature in the rubbery region, +26°C, and at two temperatures in the transition range, -45°C, -75°C. The onset of the glassy region for this material was determined to be -85°C. Tests were conducted at the following frequencies: 4×10^{-4} Hz, 2.5×10^{-3} Hz, 8×10^{-2} Hz, and at two pressure amplitudes. These loading conditions were sufficiently slow so the assumption that inertia effects are absent, i.e. the deformation is quasi-static, was effectively realized in the experiments.

The tensile specimens were cast as straight lengths of synthetic rubber 100 mm long having square cross sections with 10 mm sides. End tabs were bonded directly to the specimens so the actual length could be taken as the effective gauge length and the extension of the machine crosshead would determine the axial extension ratio λ_1. Some measurements were also taken of the change in cross section dimensions which is directly related to λ_2. Tensile tests were conducted in an Instron machine at the same temperatures as the sphere tests and at crosshead extension

rates of 0.02, 2.0 and 20 cm/min. Division by the initial length of 10 cm. would give the initial axial deformation rates.

In [10], it was reported that two terms in the series expression for $(\underline{\sigma}^a_{ij})_2$, Eq. (13), were necessary to obtain good representation for the two decades of frequency of the sphere tests. This led to five material constants in the anelastic stress term, Eq. (14), namely, α_1, α_2, g_1, g_2 and f at each temperature. In addition, the usual two elastic constants have to be specified. These seven constants were chosen to give good correspondence between the experimental and calculated results. The same material constants also led to accurate predictions of uniaxial stress-strain curves with the modification that the parameter β_2 in the W_s expression had to be non-zero to match the large strain response. As mentioned previously, a non-zero β_2 did not influence the calculations for the sphere problem which were limited to relatively low strains (about 5%). In the rubbery region, +26°C, it was found that a non-zero coupling factor γ, Eqs. (8) and (9), was more suitable to obtain good correspondence. As mentioned previously, the shear modulus μ_0 was taken to have a constant value at all the test temperatures while the Lamé coefficient λ was taken to be the same at 26°C and -45°C but differed at -75°C near the glass transition temperature. The values of the various material constants that lead to good correspondence between the test and calculated results for both the sphere and uniaxial geometries are listed in Table 1.

Results for the pressure-inner radial displacement relation for the thick walled sphere at -75°C are shown in Fig. 1 for the three frequencies. The experimental results are shown by the

continuous curves while the calculated points are indicated by symbols. Other results for the sphere problem are given in Figs. 2,3,4 at the other test temperatures. The tests at +26°C in the rubbery region, Fig. 4, show the essential absence of anelastic effects at that temperature. Unusual behavior was observed at -45°C at a frequency of 4×10^{-4} Hz, Fig. 3, which was corroborated by the calculations.

Experimental uniaxial stress-strain results at -75°C and -45°C are given in Figs. 5 and 6. On these graphs, the stress is the "true" stress based on the calculated current cross-sectional area and the indicated strain is the Cauchy axial strain or $\lambda_1 - 1$. The loading part of the curves are shown in Figs. 5 and 6 while Fig. 7 shows a more detailed picture of the calculated loading and unloading paths at -75°C for strains up to 10%. Calculations were also performed at the -75°C condition for the change of Poisson's Ratio ν with strain at two loading rates, Fig. 8, where ν is defined as

$$\nu = \frac{\Delta\lambda_2}{\lambda_2} \Big/ \frac{\Delta\lambda_1}{\lambda_1} \, . \tag{15}$$

It is noted that ν decreases with both increasing deformation rate and strain. The value of ν at zero loading rate and strain would be given by the standard elastic relation $\nu = \lambda/2(\lambda+\mu_0)$ which, for the constants listed in Table 1 at -75°C, would give $\nu = 0.362$.

Discussion

The computed deformation response for the spherical and uniaxial geometries based on the analytical formulation showed fairly good agreement with the experimental results over the range of frequencies and temperatures of the program as shown in Figs. 1-6. Although only some typical results are shown in these diagrams, the sphere tests were performed for two different sets of specimen dimensions at two maximum pressure levels for each set with equally good correspondence [18]. It was found that the constitutive equations are capable of reproducing the various phenomena that were introduced, namely nonlinear rate dependent response and energy dissipation (hysteresis) upon unloading. Figs. 1, 2, and 5 show rate dependent response for both geometries while anelasticity is indicated in the loading-unloading curves of Figs. 1, 2, 3, and 7.

The main type of nonlinearity inherent in this study is of the "magnitude" type as defined in [1] and [2]. Linear viscoelastic behavior leads to the relation

$$W_d \alpha (\sigma_a)^2 \tag{16}$$

where σ_a is the maximum amplitude of the anelastic stress in cyclic loading. For the anelastic stress equation, Eq. (14), and the material constants given in Table 1 at -75°C, the value calculated for the power in Eq. (16) for the sphere tests shown in Fig. 1 would be 2.3 which indicates magnitude nonlinearity.

Another result related to this type of nonlinearity is obtained by comparing results of calculations based on classical linear elasticity with the nonlinear elastic formulation of the

sphere problem. At circumferential strains up to about 5% the deviation between the linear and nonlinear results is small while at 10% strain the deviation rises to about 20%.

A further aspect of nonlinear behavior is found from the time dependence of the constant strain rate uniaxial tests. It is found (from the isochronic data of Table 2) that the stress at given times does not depend linearly on the velocity. The data in Table 2 for tests at -75°C indicates that the response is close to linear up to 0.2 minutes, after which it becomes nonlinear from 0.4 to 2 minutes and subsequently reapproaches linearity after about four minutes.

Rate dependent response is shown in both the pressurized sphere and uniaxial tension tests. In both types of experiments the effective modulus increases with loading frequency or axial velocity. The material parameters in the constitutive equation responsible for this behavior are: α_1, α_2, g_1, g_2. These were determined to fit the pressurized sphere tests and were then applied to the uniaxial tension tests. Good matching is achieved in both types of loading, e.g. Figs. 1, 2, 5 and 6.

The damping loss factor is defined by Eq. (11). It is interesting to note that it does show some frequency dependence due to nonlinear interactions. The computed values of the loss factor for the pressurized spheres at -75°C and at a peak pressure of 10 N/cm^2 are: 0.21, 0.28, and 0.26 at the loading frequencies of 4×10^{-4}, 2.5×10^{-3}, and 8×10^{-2} Hz respectively. These values agree well with damping measurements of low amplitude free vibration torsion tests carried out at comparable frequencies. At a peak pressure of 40 N/cm^2 the computed loss factors at the same three frequencies are: 0.072, 0.096 and 0.088

which shows an overall decrease with increasing amplitude.

Uniaxial tension tests were performed only in loading (no unloading). However, the computed results, Fig. 7, do show that the hysteresis loop area, and therefore tan δ, depends on the imposed velocity for this loading mode as well. Again it is observed that tan δ decreases with increasing rate of deformation.

The calculated values of Poisson's Ratio, Fig. 8, also show a deformation rate dependence. We do not have experimental values to compare to the calculated ones, but another investigation on dilatometric properties of a similar rubber [17] showed a similar trend for Poisson's Ratio. That is, a decrease in deformation rate resulted in higher values of Poisson's Ratio corresponding to smaller volumetric changes during extension tests. Poisson's Ratio is also strain dependent which is shown in the calculated results of Figure 8.

The response of the tested material is observed to be more rigid near the origin of the stress-strain curve than at large strains. This is expressed by a steep slope near the origin, e.g., Figs. 1, 2, 5, 7. In the calculations, this is a consequence of the friction term in the anelastic stress expression.

In the pressurized sphere tests, unusual behavior was observed at -45°C and a frequency of 4×10^{-4} Hz in both the tests and the calculated results, Figure 3. The calculated amplitude at which hysteresis disappears is controlled by the coefficient g_2. The reason for this behavior is not clear but the fact that it is obtained experimentally and is also predicted by the analytical formulation is an indication of the representation capability of the theory.

Good matching of the uniaxial experimental results up to about 40% strain at -75°C and 100% at -45°C could be obtained through the modification of the elastic distortion energy W_s by including a non-zero value for the β_2 coefficient. With $\beta_2=0$, matching is limited to strains of only 15% at -75°C. It seems that the restriction to fitting results with the more general expression for W_s, Eqs. (6) and (7), lies in its monotonic nature. The material stress-strain curve at -75°C is characterized by an inflexion point which could be accomodated if the elastic shear energy function, W_s, consisted of polynomials higher than the second. It could then allow matching of stress-strain curves having inflexion points as well. Such functions will, however, require a large number of coefficients which will create computational and experimental problems in their adequate determination. It therefore seems that inflexion points of the stress-strain curve impose the practical limit of application of the present theoretical model.

The uncoupled strain energy form was found to result in good matching of experimental and calculated results in the transition region (-45°C, -75°C). However, in order to obtain good matching of the detailed test results for both sets of sphere specimens and for the uniaxial specimens in the rubbery region, 26°C, the coupled energy form had to be used. At that temperature, the pressure-radial displacement curves of the thinner walled spheres (75mm - 100mm diameter) and the uniaxial stress-strain curves were extremely steep at the origin. This behavior can be predicted from the calculations by the use of the coupled form of the strain energy function.

In conclusion, the overall results show that the representation capability of the analytical model is fairly good for most engineering purposes. The mathematical formulation is relatively simple and enables accurate determination of the material parameters. Since the constitutive equations are in differential form, they can be readily incorporated into numerical procedures for solving stress analysis problems by step by step methods. The results obtained for both the spherical and uniaxial geometries encourage the continuation of testing and evaluation of the theoretical model.

References

1. F.J. Lockett, Nonlinear Viscoelastic Solids, Academic Press, 1972.
2. F.J. Lockett, Proc. IUTAM Symp. on Mechanics of Visco-Elastic Media and Bodies, Springer, 1 (1975).
3. M.E. Gurtin and E. Sternberg, Arch. Ration. Mech. Anal., 11, 291 (1962).
4. R.S. Rivlin, Proc. IUTAM Symp. on Mechanics of Visco-Elastic Media and Bodies, Springer, 26 (1975).
5. C.M. Zener, Elasticity and Anelasticity of Metals, Univ. Chicago Press, 1948.
6. Y. Partom, Inter. J. Non-Linear Mech., 5, 475 (1970).
7. S.R. Bodner and Y. Partom, J. Appl. Mech., 39, 751 (1972).
8. S.R. Bodner and Y. Partom, J. Appl. Mech., 42, 385 (1975).
9. F.J. Lockett, NPL Report Mat. Appl. 36, August 1974.
10. D. Derman, S.R. Bodner and Y. Partom, Proc. IUTAM Symp. on Mechanics of Visco-Elastic Media and Bodies, Springer, 196 (1975).
11. Y. Partom, D.Sc. dissertation, Technion - Israel Institute of Technology, 1967.
12. A.C. Eringen, Nonlinear Theory of Continuous Media, McGraw-Hill, 1962.
13. Y. Partom, Israel J. Tech., 4, 218 (1966).
14. A.M. Freudenthal and H. Geiringer, Handbuch der Physik, Springer-Verlag, 6, 258 (1958).
15. J.D. Ferry, Viscoelastic Properties of Polymers, John Wiley & Sons, 1961, p. 410.
16. B. Hartmann and J. Jarzynski, J. Appl. Phys., 43, 4304 (1972).
17. Y. Diamant (Haifa), private communication.
18. D. Derman, D.Sc. dissertation, Technion - Israel Institute of Technology, 1973.

List of Captions

Fig. 1 - Experimental and calculated results for the pressure-inner radial displacement relation of a thick walled synthetic rubber sphere at -75°C.

Fig. 2 - Experimental and calculated results for the pressure-inner radial displacement relation of a thick walled synthetic rubber sphere at -45°C.

Fig. 3 - Experimental and calculated results for the pressure-inner radial displacement relation of a thick walled synthetic rubber sphere at -45°C and 4×10^{-4} Hz.

Fig. 4 - Experimental and calculated results for the pressure-inner radial displacement relation of a thick walled synthetic rubber sphere at 26°C.

Fig. 5 - Experimental and calculated uniaxial stress-strain curves for a synthetic rubber at -75°C.

Fig. 6 - Experimental and calculated uniaxial stress-strain curves for a synthetic rubber at -45°C.

Fig. 7 - Calculated uniaxial loading and unloading stress-strain relations for a synthetic rubber at -75°C.

Fig. 8 - Calculated dependence of Poisson's Ratio on crosshead velocity and strain for a synthetic rubber at -75°C.

TABLE 1

Material Constants

Temperature	Shear Modulus	Lamé Coeff.	Shear Energy Parameters		Coupling Factor	Friction Parameter	Coefficients		Rate Coefficients	
T	μ_e	λ	β_1	β_2	γ	f	g_1	g_2	α_1	α_2
°C	N/cm^2	N/cm^2				N/cm^2			$(sec)^{-1}$	$(sec)^{-1}$
26	110	400	1/9	0	50	8×10^{-4}	0	0	0	0
-45	110	400	-0.3635	1.425	0	0.023	0.25	0.05	5×10^{-5}	5×10^{-7}
-75	110	290	-0.9123	3.065	0	0.4	1.2	0.35	5×10^{-5}	5×10^{-7}

TABLE 2

Isochrones from Uniaxial Tests at -75°C.

True stress [kg/cm^2] after a period of minutes:					Cross Head Speed [cm/min]
4	2	0.4	0.2	0.1	
0.45	0.232	0.056			0.02
45.4	21.2	5.06	2.83	1.60	2.0
		58.5	28.0	16.3	20.0

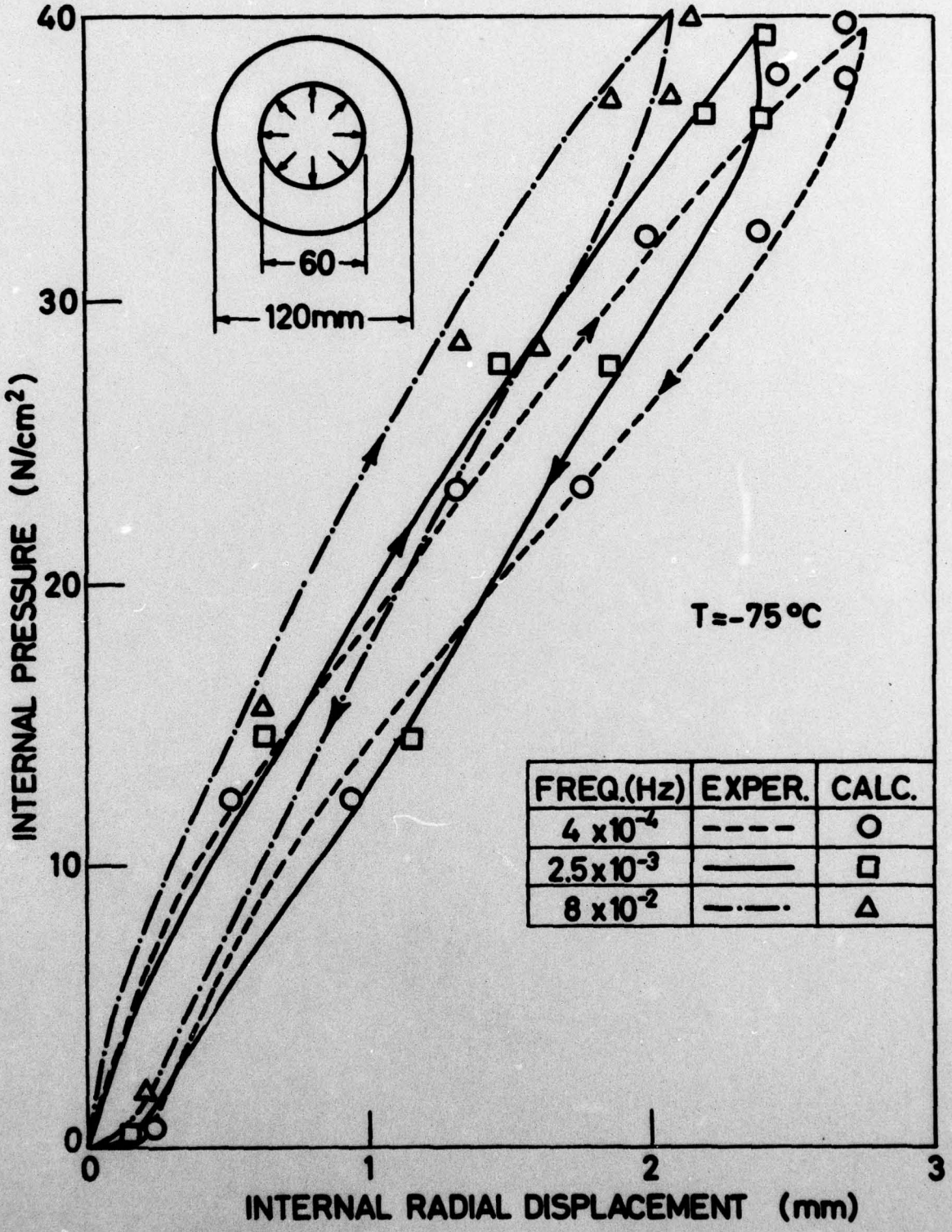
40
30
20
10
0
0
1
2
3
INTERNAL PRESSURE (N/cm²)
INTERNAL RADIAL DISPLACEMENT (mm)
60
120mm
T=-75°C
FREQ.(Hz)
EXPER.
CALC.
4 x10⁻⁴
2.5x10⁻³
8 x10⁻²

FIG. 1

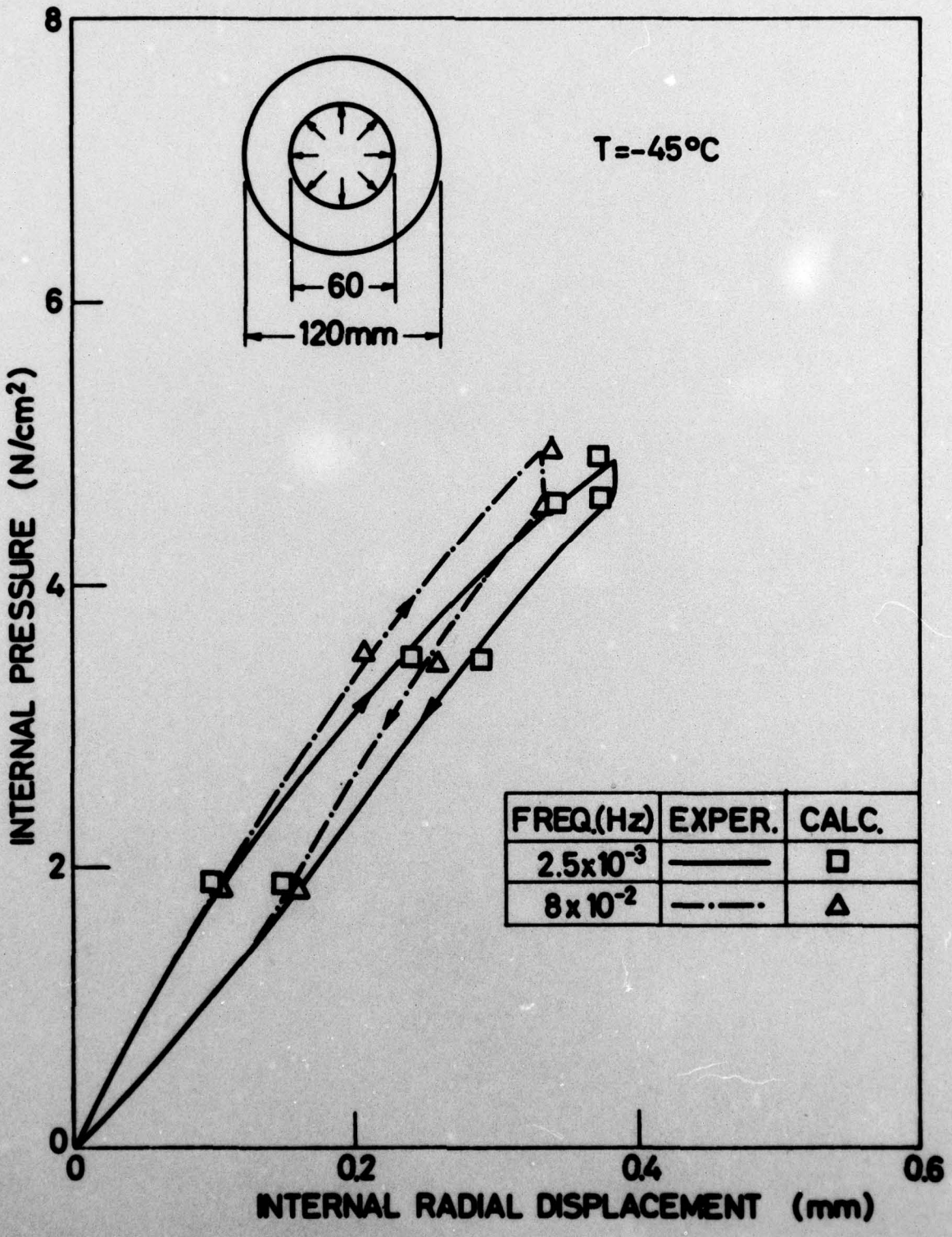
8
6
4
2
0
INTERNAL PRESSURE (N/cm²)
60
120mm
T=-45°C
FREQ.(Hz)
EXPER.
CALC.
2.5x10⁻³
8x10⁻²
0
0.2
0.4
0.6
INTERNAL RADIAL DISPLACEMENT (mm)

FIG. 2

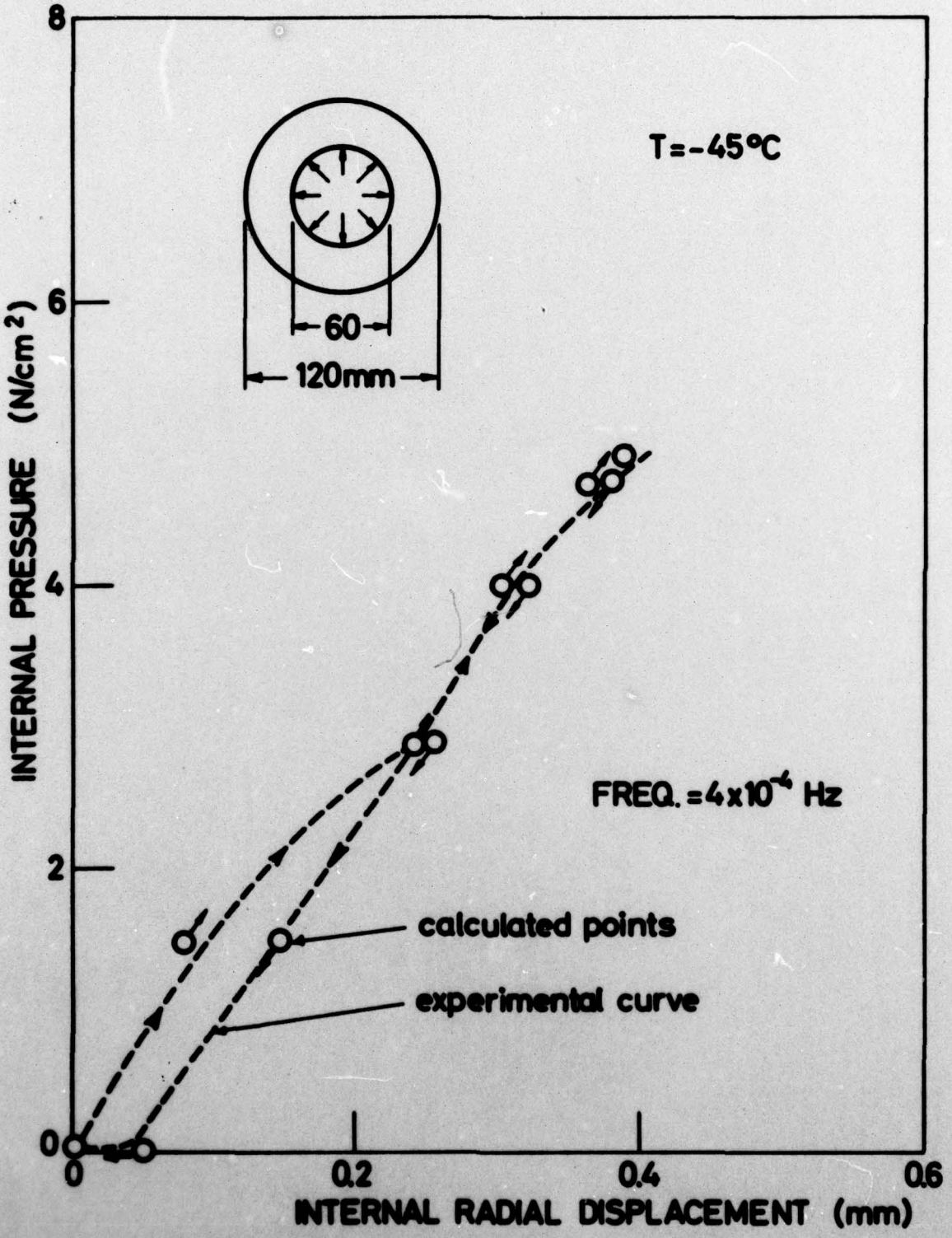
8
6
4
2
0
0
0.2
0.4
0.6
INTERNAL PRESSURE (N/cm²)
INTERNAL RADIAL DISPLACEMENT (mm)
T=-45°C
60
120mm
FREQ. =4x10⁻⁴ Hz
calculated points
experimental curve

FIG. 3

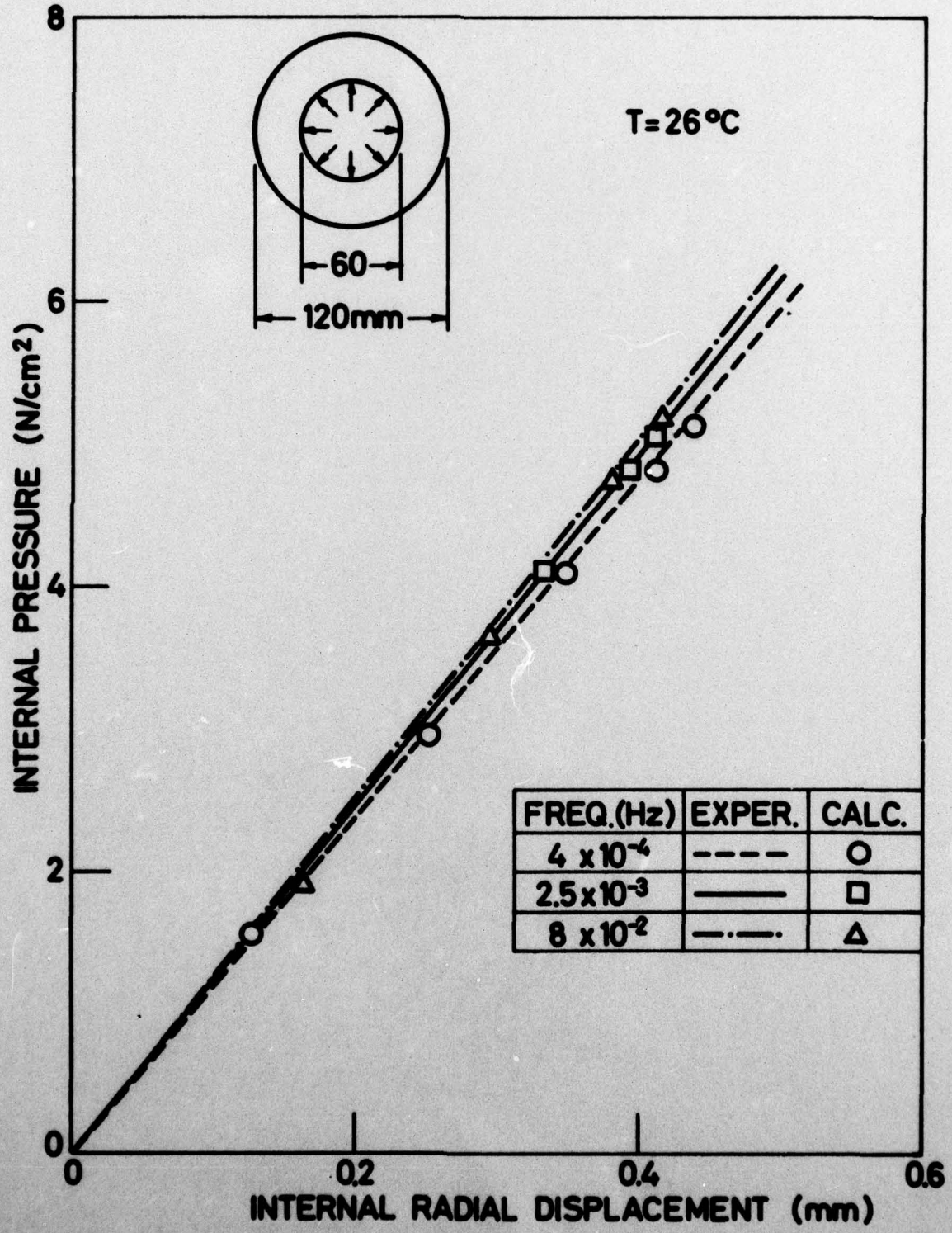
8
6
4
2
0
INTERNAL PRESSURE (N/cm²)
T=26°C
60
120mm
FREQ.(Hz)
EXPER.
CALC.
4 x10⁻⁴
2.5x10⁻³
8 x10⁻²
0
0.2
0.4
0.6
INTERNAL RADIAL DISPLACEMENT (mm)

FIG. 4

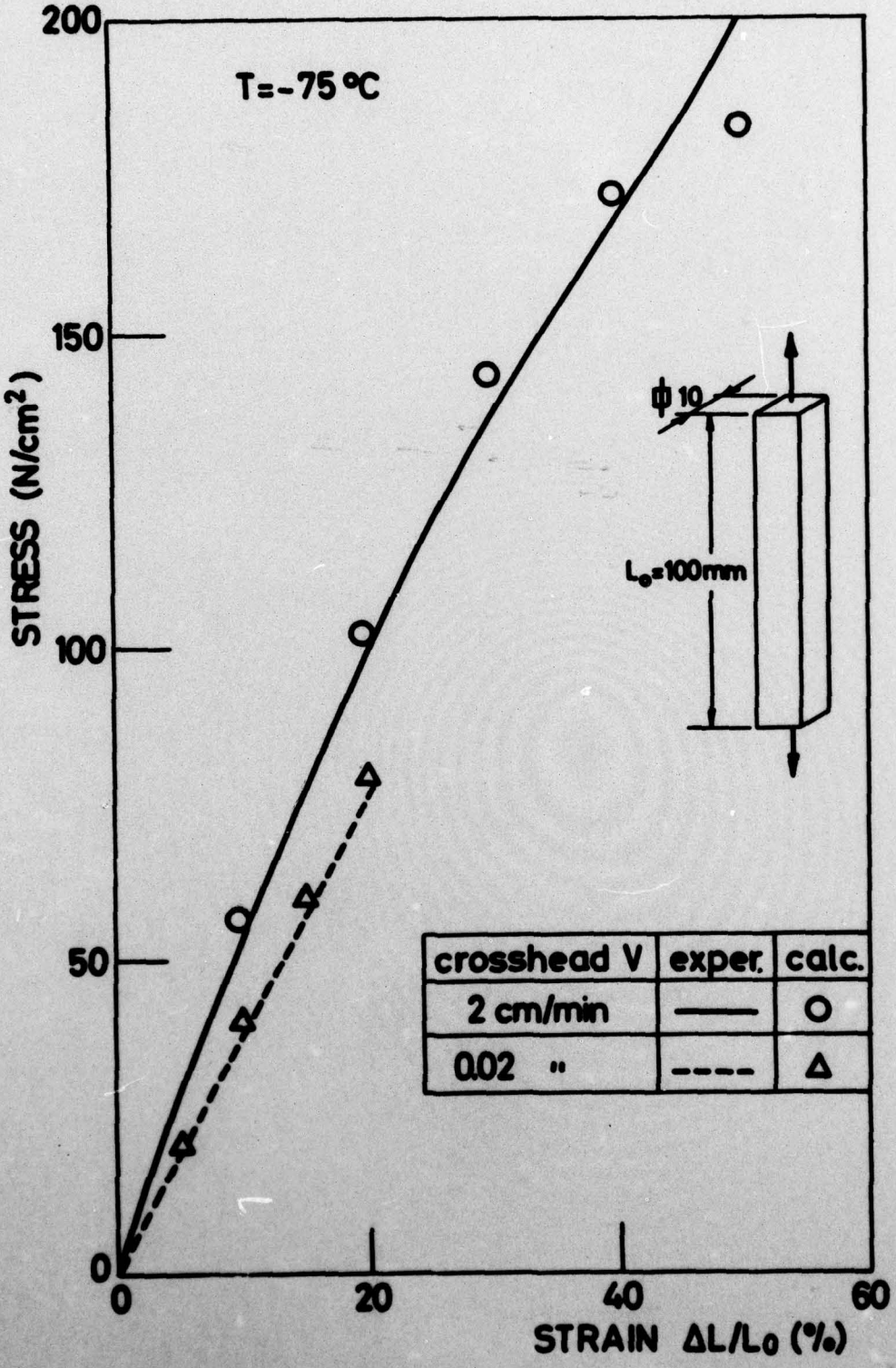
T=-75 °C
STRESS (N/cm²)
200
150
100
50
0
0
20
40
60
STRAIN ΔL/L₀ (%)
φ 10
L₀=100mm
crosshead V
exper.
calc.
2 cm/min
0.02 "

FIG. 5

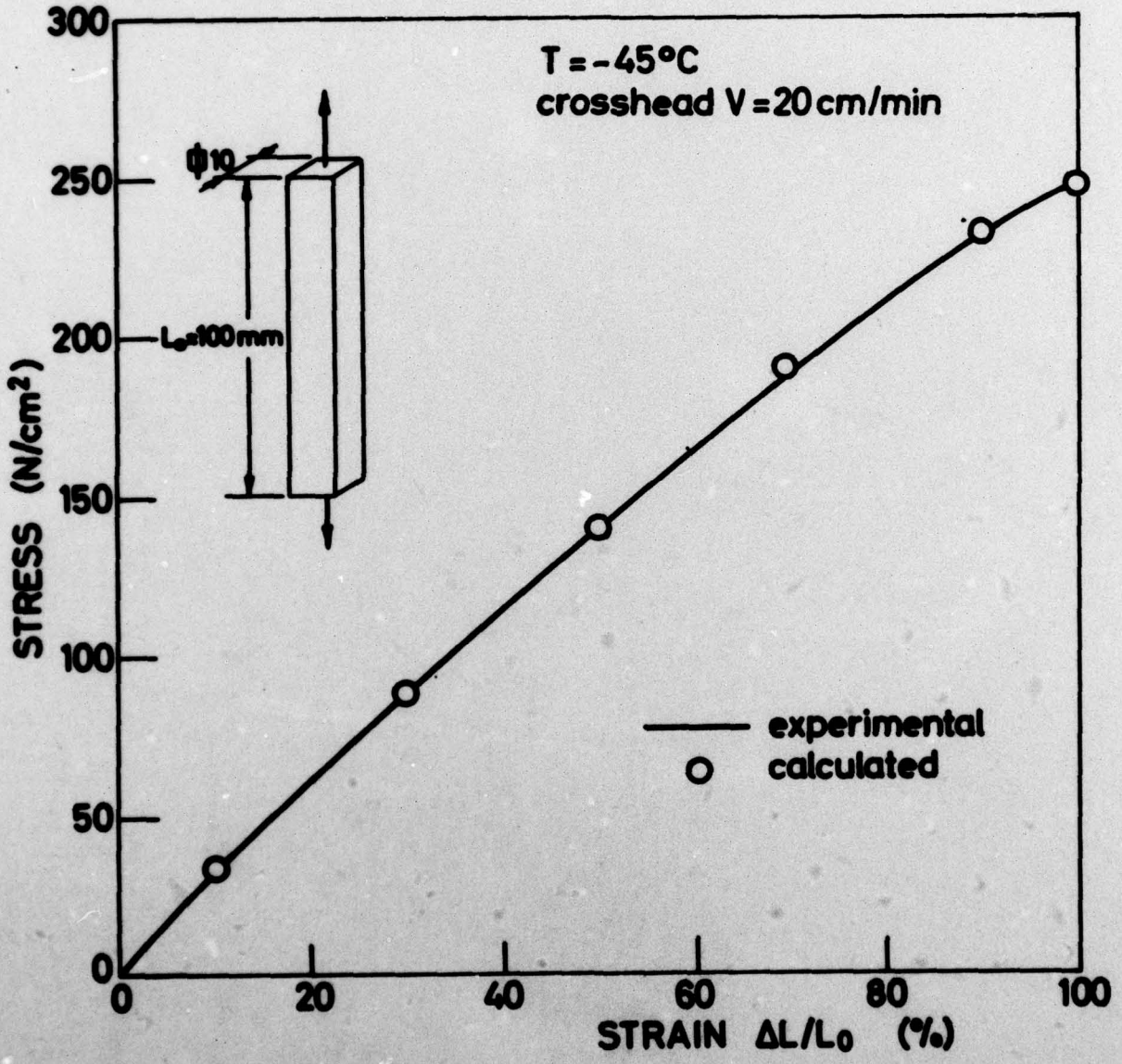
T = -45°C
crosshead V = 20 cm/min
φ10
L₀=100mm
STRESS (N/cm²)
300
250
200
150
100
50
0
0
20
40
60
80
100
STRAIN ΔL/L₀ (%)
experimental
calculated

FIG. 6

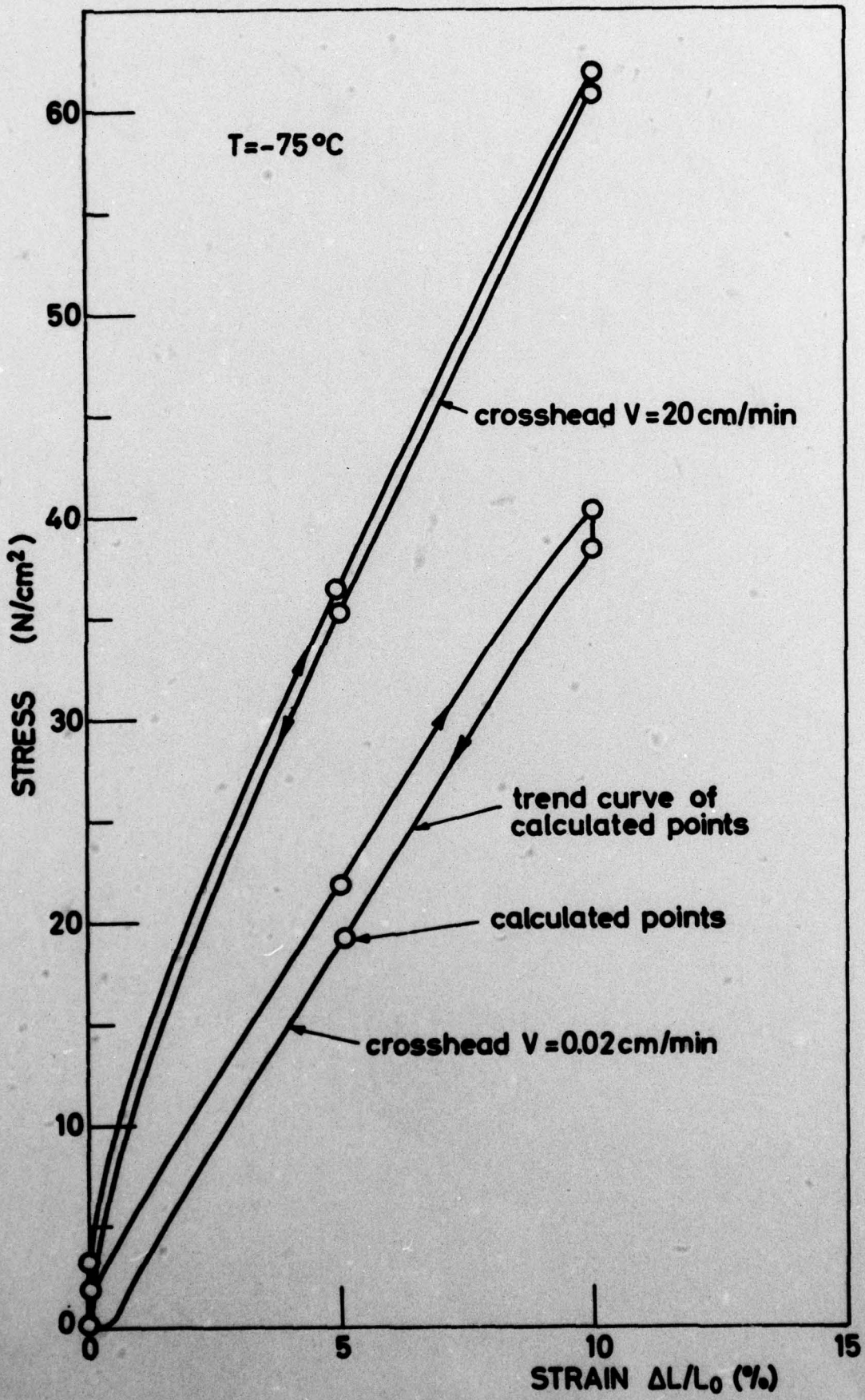
T=-75°C
crosshead V=20cm/min
trend curve of calculated points
calculated points
crosshead V=0.02cm/min
STRESS (N/cm²)
STRAIN ΔL/L₀ (%)
0
10
20
30
40
50
60
0
5
10
15

FIG. 7

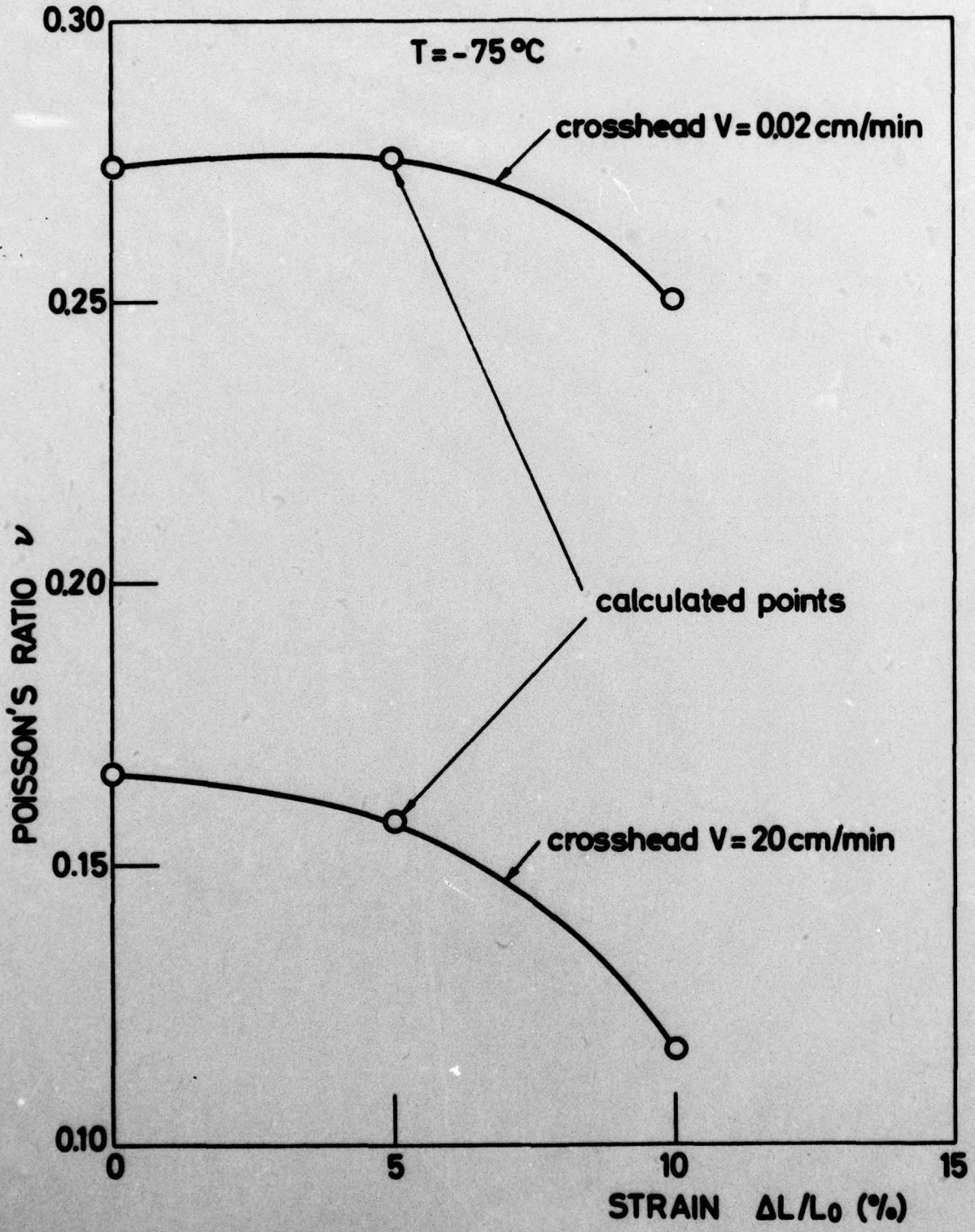
T = -75 °C
crosshead V = 0.02 cm/min
calculated points
crosshead V = 20 cm/min
POISSON'S RATIO ν
0.30
0.25
0.20
0.15
0.10
0
5
10
15
STRAIN ΔL/L0 (%)

FIG. 8